GEOLOGIE EN MIJNBOUW© VOLUME 57 (4), p. 487-502 1978

MAGNESIUM-SALT EXPLORATION IN THE NORTHEASTERN NETHERLANDS

P. A. J. COELEWIJ[1], G. M. W. HAUG[2] & H. VAN KUIJK[3]

ABSTRACT

Coelewij, P. A. J., G. M. W. Haug & H. van Kuijk (1978). Magnesium-salt exploration in the northeastern Netherlands. *In:* A. J. van Loon (ed.): Key-notes of the MEGS-II (Amsterdam, 1978). Geol. Mijnbouw, 57, p. 487-502.

Magnesium-bearing salts occur in the Zechstein Basin in the northeastern Netherlands at a depth of 1500 to 2500 m. Exploration has resulted in the discovery of significant amounts of this salt which will be exploited by solution mining for the production of refractory grade magnesiumoxide. Of the four main evaporite cycles, Zechstein III (the ore-bearing cycle) is fully developed and contains the magnesium salts carnallite ($MgCl_2.KCl.6H_2O$), bischofite ($MgCl_2.6H_2O$) and kieserite ($MgSO_4.H_2O$).

The salt sequence has been affected by halokinesis, resulting in salt domes and other structures. The magnesium-bearing layers were thickened towards the top of the structures, thus forming prime targets for exploration. Exploration techniques comprise seismic surveys and rotary drilling. Conventional seismic methods adequately define depth and structural configuration, whilst high-resolution seismic wavelet processing is used for the identification of the magnesium-salt layers on the seismic section and determination of thickness. Seismic sections are converted into acoustic impedance sections which are calibrated from acoustic impedance logs. These in turn are derived from velocity and density measurements in bore holes.

The mineral composition, ore grade, and thickness can be accurately determined by petrophysical well-logging: in particular formation density, gamma ray, and sonic logs. Results are calibrated by chemical analysis of drillcores.

INTRODUCTION

Billiton International Metals B.V., a wholly owned company of the Royal Dutch Shell Group, is active in metal exploration, mining, processing, and trading. The company has defined certain priority metals, mainly in the non-ferrous sector, in which it intends to become increasingly involved to augment its present activities: one of these is magnesium.

Magnesium ores can be used for the production of metal, chemical, industrial or pharmaceutical products, and for refractories. Billiton has decided to become active initially in the field of refractory materials by producing high-grade magnesium oxide, which is used mainly in the steel industry for the lining of furnaces. An extensive exploration programme has been carried out to locate raw material for the production of magnesium oxide. The following chapters describe this programme and results obtained to date.

[1] Head, Metals Exploration, Billiton International Metals B.V., THE HAGUE, The Netherlands.
[2] Senior Geologist, Billiton International Metals B.V., THE HAGUE, The Netherlands.
[3] Senior Geophysicist, Shell Internationale Petroleum Mij. B.V., THE HAGUE, The Netherlands.

MAGNESIUM RAW MATERIAL

The main categories of magnesium raw material are listed in Table I.

Table I
Main categories of magnesium raw-material.

MAGNESIUM SOURCES	A. ULTRABASIC IGNEOUS ROCKS 1. carbonates 2. silicates (magnesite, talc) B. SEDIMENTARY ROCKS 1. carbonates (magnesite, dolomite) C. EVAPORITES 1. chlorides 2. sulphates (carnallite, bischofite, kieserite) D. SEA WATER

To produce high-grade magnesium oxide, Billiton has selected the evaporite category as the primary source. Hardrock resources like magnesite ($MgCO_3$) and dolomite ($CaMg(CO_3)_2$) contain relatively high amounts of impurities like iron, silica and alumina, which are costly to remove, whilst seawater has a relatively high boron content.

Magnesium salts of economic interest occurring in evapo-

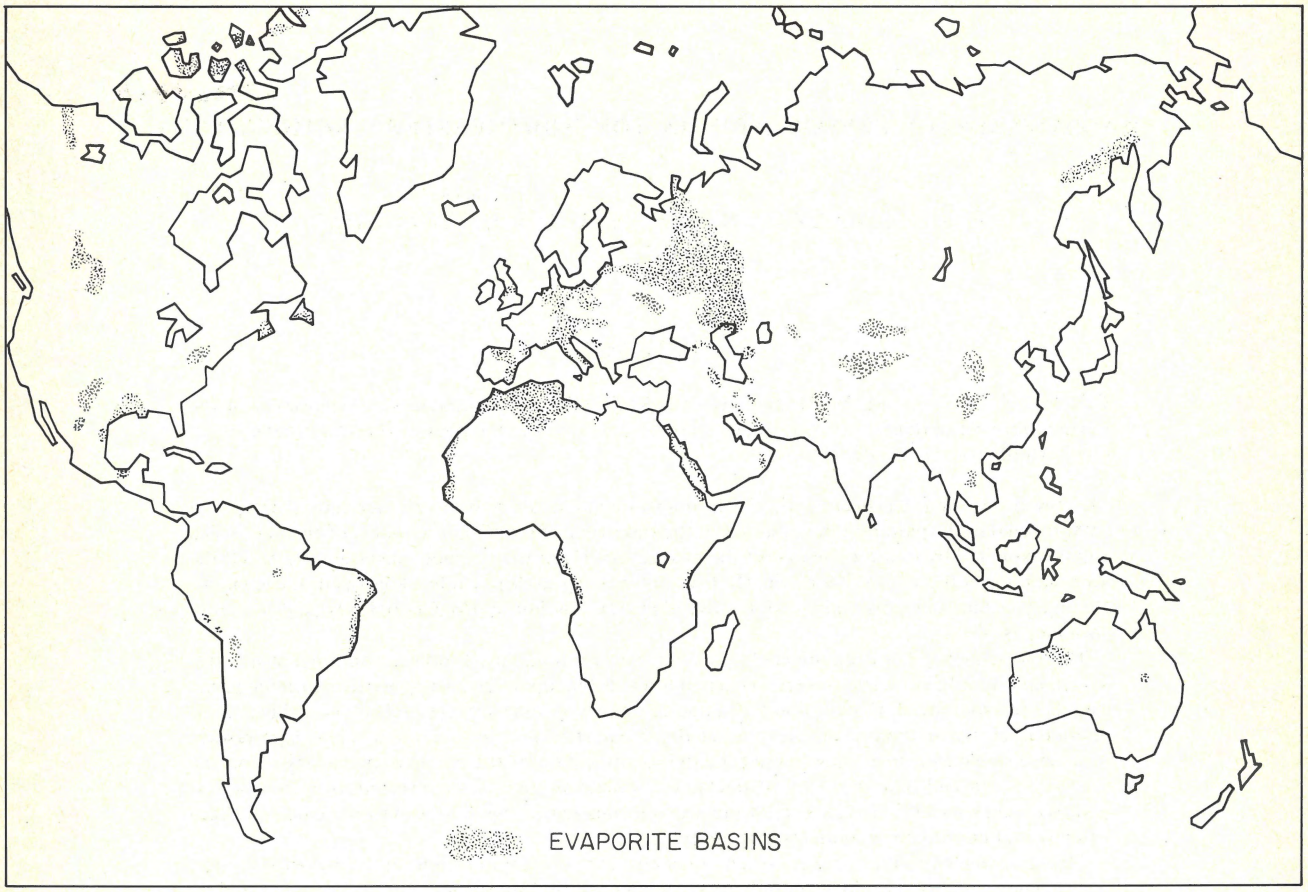

Fig. 1
Distribution of evaporite basins.

rite deposits are (percentages by mass):

(1) carnallite — $KCl.MgCl_2.6H_2O$ → 8,75% Mg
(2) bischofite — $MgCl_2.6H_2O$ → 11,96% Mg
(3) tachyhydrite — $MgCl_2.CaCl_2.12H_2O$ → 9,40% Mg
(4) kieserite — $MgSO_4.H_2O$ → 17.57% Mg

The first two have wide distribution and occur in many evaporite basins. Tachydrite has been found in large quantity in evaporite basins in Gabon and Brazil, whilst kieserite usually accompanies carnallite, albeit as a minor constituent.

EXPLORATION CRITERIA

Following the decision to exploit magnesium salts, Billiton carried out a worldwide study of evaporite basins in order to develop a thorough knowledge on which to base selection of the most attractive area for exploration. Figure 1 shows schematically the distribution of major evaporite basins of Palaeozoic to Recent age; a large number have considerable extensions offshore which are not shown on the map.

The study of evaporite basins taught that four geological criteria are significant in selecting exploration ground. These are:

(1) the development, configuration and sedimentary environment of the basin during deposition of the evaporites;
(2) halokinesis and the degree of development of salt structures;
(3) post-depositional tectonism, and local disturbances;
(4) the effect of erosion and leaching of salt throughout the geological history.

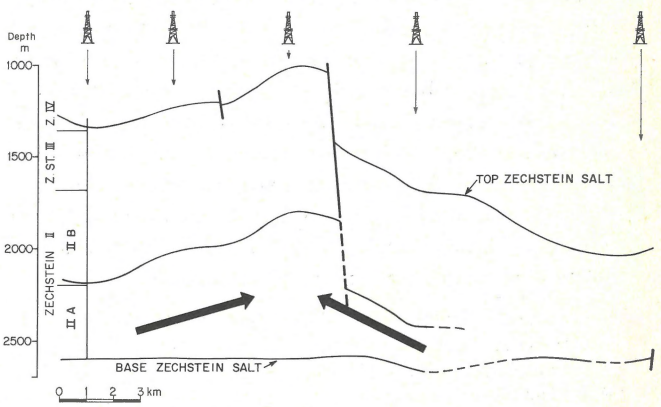

Fig. 2
Differential flow in rock salt.

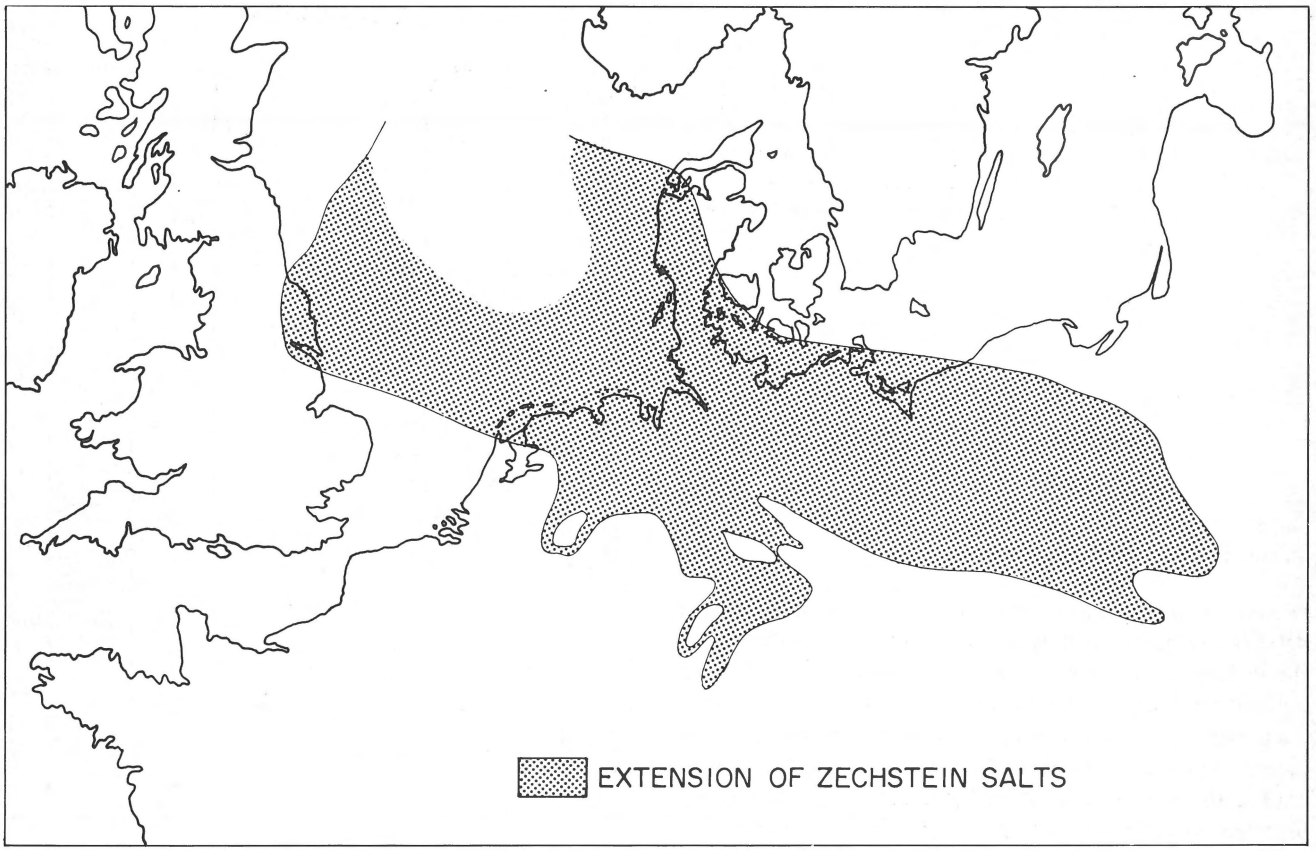

Fig. 3
Salt extension of the Zechstein Basin.

The sequence of deposition in an evaporite cycle is carbonate, anhydrite, halite, carnallite and, in the case of a full cycle, bischofite. Magnesium salts represent the last phase in the evaporation and therefore occur usually in the upper part of the sequence and towards the centre of the basin, where prospectivity naturally increases.

The phenomenon of halokinesis is very important. With sufficient overburden and salt thickness, instability results in an upward plastic flow of the salt. Vertical structures are formed during this process, ranging from gently sloping domes (pillows) with undisturbed roofs to salt dykes, and diapirs piercing overlying strata. Halokinesis is a complex process, especially when different salts with different physical properties are involved. The yielding stress of halite at simulated subsurface conditions (2400 m depth and 100°C), for example, is 40 kg/cm^2, whereas this value for carnallite is 4.5 kg/cm^2, and for bischofite 1.0 kg/cm^2. These values have been determined at the Shell Research laboratory at Rijswijk (The Netherlands).

From studies of evaporite basins in the world two major types of flow processes in salt can be distinguished, which the authors propose to call differential and preferential flow.

Differential flow is defined as the process of plastic flow of part of the rock salt whilst the remainder stays rigid. The degree of instability in a buried salt layer increases as a function of overburden pressure and temperature. Consequently, the process of plastic flow commences at the base of the salt sequence causing local thickening of the lower part, whereas the thickness of the upper sequence remains unaffected. This process, which is also observed in the northeastern Netherlands, is illustrated in figure 2.

Preferential flow is defined as the process of salt flow which develops when salt layers of different composition and rheological characteristics (e.g. rock salt and magnesium salt) occur within the salt sequence. In such instances salt layers of one type may be subject to plastic flow whilst the salt of different type may not.

In many salt basins, including that in the northeastern Netherlands, this resulted in the formation of bischofite/carnallite subpillows within the main salt structure. These subpillows vary in size, but are much smaller than the main salt structure; probably in the order of tens or hundreds of metres in diameter. Preferential flow may take place under conditions of temperature and pressure different to those required for differential flow. In one salt structure, therefore, both processes may occur at different times, or concurrently at different levels.

The processes of differential and preferential flow are im-

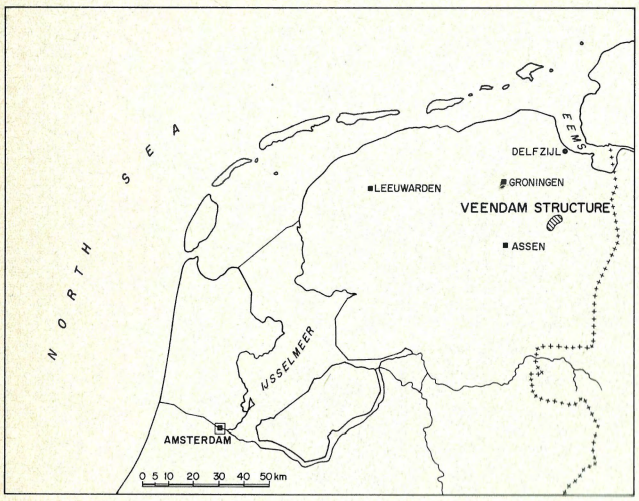

Fig. 4
Situation of the Veendam salt structure.

portant phenomena in the formation of magnesium salt ore deposits. Differential flow usually results in a shallowing of the drilling target, whilst preferential flow results in an increased thickness of the target horizon; both processes reduce exploration and mining costs. In the mining area selected (Veendam structure, Zechstein Basin, The Netherlands), the magnesium-salt horizon has been uplifted approximately 1000 m by differential flow and the thickness of the magnesium sequence has locally increased threefold as a result of preferential flow.

Another significant exploration parameter is the degree of vertical development of the salt structure formed by halokinesis and the condition of the roof. Domal upheaval and associated stretching of the roof causes tensional cracks, thereby reducing its strength and resistance to retain the salt 'enclosed' in the structure. The more developed the structure, the weaker the roof. In extreme cases the plastic salt breaks through the roof and pierces the overlying formations. Bischofite (being the most mobile constituent and occurring usually high up in the sequence) easily escapes into the overlying formations where it often dissolves in formation water and is lost. During this piercement process carnallite usually becomes complexly folded. This considerably reduces the recoverability by solution mining. Salt piercements and salt pillows with a strongly deformed roof are therefore no good targets for magnesium-salt exploration.

EXPLORATION PROGRAMME

Area

The Zechstein Basin is of Permian age and extends from the northern Netherlands to the North Sea, Germany and Poland, and covers an area of approximately 800,000 km^2 (Fig. 3). The Zechstein Basin in the northern part of The

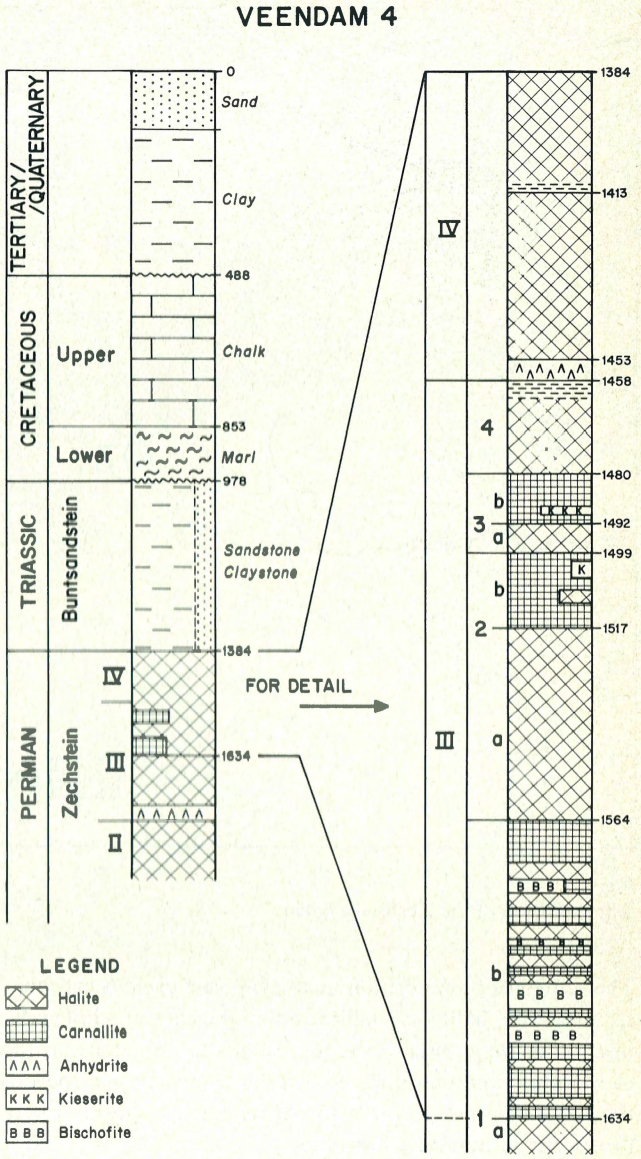

Fig. 5
Stratigraphy.

Netherlands was selected for further exploration work with the object of developing an underground mine using solution mining techniques. The selection was based on both geological and economic/political criteria.

It was known that magnesium salts occurred in the basin and that halokinesis had resulted in the formation of salt structures; the magnesium salt presumably would have been increased locally in thickness and uplifted to shallower depth.

Economically, the infrastructure, investment climate, labour situation etc. was considered good. One of the most important factors in the decision to select the northern Netherlands, however, was the proximity to markets. Western Europe is a major steel producer with the northern Netherlands favourably located in the centre.

Table II
Drillhole summary (all values in m).

				VE 1		VE 2		VE 3		VE 4	
				depth	thickness	depth	thickness	depth	thickness	depth	thickness
IV			rocksalt + clay	1363.0	62.0	1321.0	55.6	1503.4	86.1	1383.6	74.7
ZECHSTEIN III	4		rock salt	1425.0	22.4	1376.6	46.1	1589.5	18.2	1458.3	21.5
	3	b	Mg-salt	1447.4	15.1	1422.7	29.8	1607.7	8.5	1479.9	12.0
		a	rock salt	1462.5	8.1	1452.5	13.5	1616.2	6.8	1491.8	7.4
	2	b	Mg-salt	1470.6	82.0	1466.0	9,8	1623.0	12.0	1499.1	18.1
		a	rock salt	1552.6	83.9	1475.8	39.2	1635.0	45.1	1517.2	46.4
	1	b	Mg-salt	1636.5	36.5	1515.0	104.4	1680.1	54.4	1563.6	70.0
		a	rock salt	1673.0	–	1619.4	–	1734.6	–	1633.8	–
	cumulative thickness Mg-salt layers			–	133.6	–	144.0	–	74.9	–	100.1

History

In order to establish the presence of magnesium salts, and to verify the validity of the theory of differential and preferential salt flow in the Dutch part of the Zechstein Basin, a hole was drilled in 1972 in the Veendam salt-structure near Groningen (Fig. 4). According to the expectation, magnesium salts (carnallite, bischofite and kieserite) were intersected at three intervals within the Zechstein at about 1400 m depth, with a total net thickness of 133.6 m.

Table III
Primary features in subcycles Z-III-2+3-b versus subcycle Z-III-1-b.

	Zechstein-III-1-b	Zechstein-III-2+3-b
Cyclic development	Nine sub-subcycles distinguished, of which each contains a large number of mini-cycles.	No distinct cycles present.
Bedding	Distinct bedding present, normally mono-or bimineral composition.	Indistinct bedding; normally coarse crystalline mixture.
Colour	Always milky white to translucent, colourless.	Predominantly red carnallite and translucent, colourless halite; latter red at top of Z-III-3-b
Mineralogy	Halite, kieserite, carnallite, bischofite; accessory anhydrite, locally some clay.	Halite, kieserite, carnallite; accessory anhydrite.

Having established the presence of a substantial magnesium-salt occurrence, the exact size and shape of the salt structure, the deformation of the roof and the post-depositional geological history were investigated in 1975. For this purpose a seismic survey was carried out over the structure. Apart from traditional seismic work, primarily directed towards the acquisition of structural information, a new method of data processing was applied to test the application of acoustic impedance interpretation (lateral prediction) for the identification of magnesium salts and determination of thickness variations.

Initial results were favourable and in the next phase three additional boreholes were drilled to further establish the configuration and grade of the ore, and to estimate reserves. These holes were drilled in 1976 and are pending completion for production.

Late in 1978, a 3-dimensional high-resolution seismic survey will be carried out, to delineate subsurface magnesium-salt subpillows. This will allow determination of reserves in the mining area, and the selection of production well locations.

EXPLORATION RESULTS

Stratigraphy

The history of Zechstein evaporite basin in the northeastern Netherlands comprises four main cycles (I-IV), of which cycle III is fully developed and contains magnesium salt at the top.

The evaporites are covered with younger sediments of Triassic, Cretaceous, Tertiary and Quarternary age, varying in thickness from 1500 to 2500 m.

The stratigraphy of the Zechstein evaporite sequence and

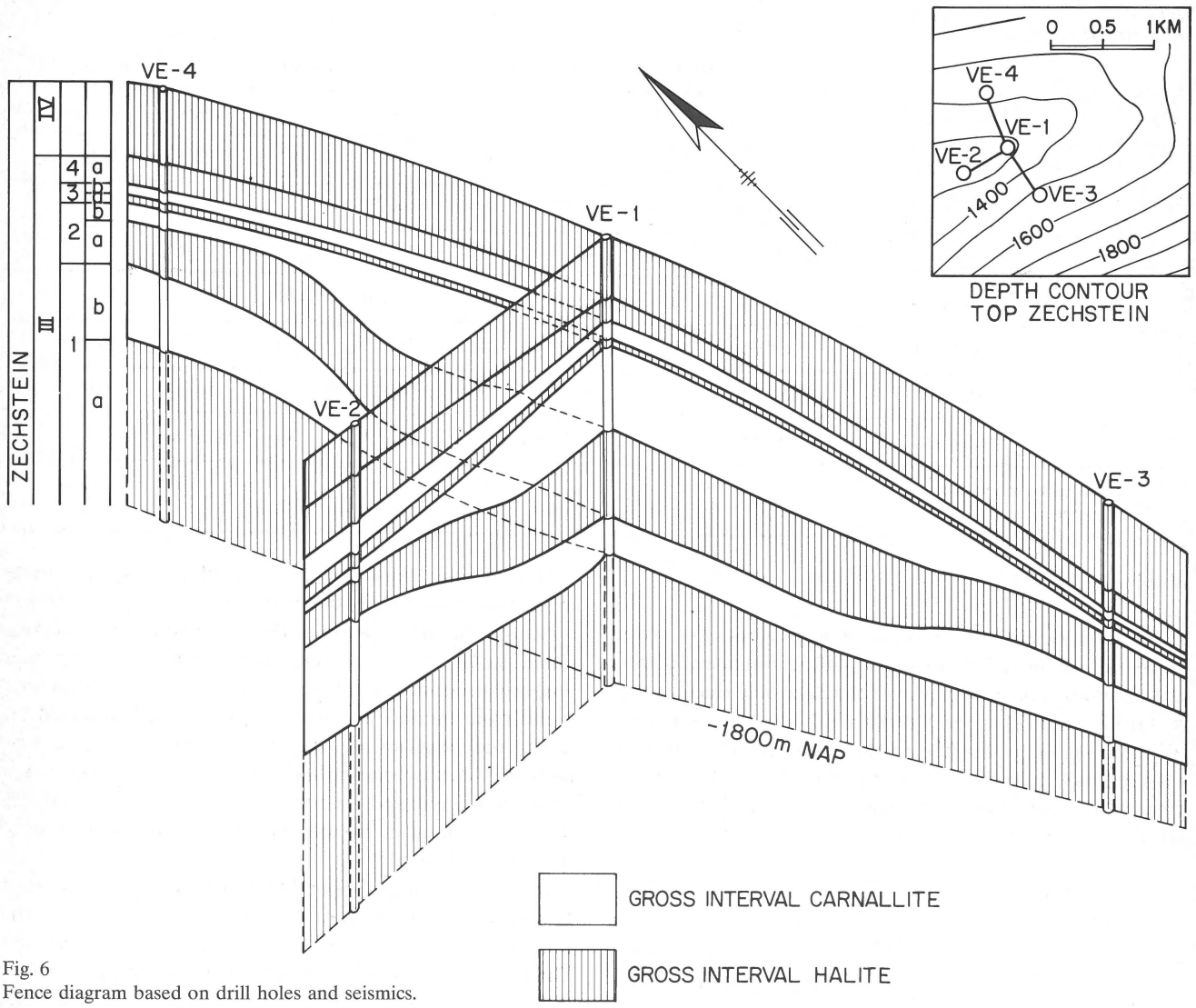

Fig. 6
Fence diagram based on drill holes and seismics.

the overlying strata is shown in figure 5. In the Zechstein III cycle four subcycles are distinguished: Z-III-1, 2, 3 and 4. They contain a lower rock-salt unit, and except for Z-III-4, are followed by a carnallite layer at the top. The lowest subcycle (Z-III-1) also contains bischofite.

The summary drill-hole table (Table II) gives the depth and intersected thicknesses of the cycles in the four drill-holes. The large differences in thickness of magnesium salts are ascribed to the process of preferential salt flow discussed before.

Correlation of subcycles in Zechstein III between the four drillholes is shown on the fence diagram (Fig. 6). The lower subcycle (Z-III-1), developed in the Veendam area, correlates with the Ronnenberg horizon and the two upper subcycles (Z-III-2 and Z-III-3) with the Riedel horizon in Germany.

Drill-cores from Zechstein III are shown on figure 7.

Flow features are common and dips measured on the cores do not necessarily represent the regional dip of the structure. Recrystallisation of carnallite and bischofite have locally obliterated bedding planes where crystals of 15-30 mm have been developed. Competent halite and kieserite beds within thick carnallite react to preferential flow by folding and rupture.

Table IV
Temperature of primary precipitation (from Braitsch, 1971, p. 259).

temperature	25°C	35°C	55°C
1. kieserite	40%	29.5%	6.5%
2. carnallite	48%	59%	86.5%
Ratio kies./carn.	0.83	0.5	0.075

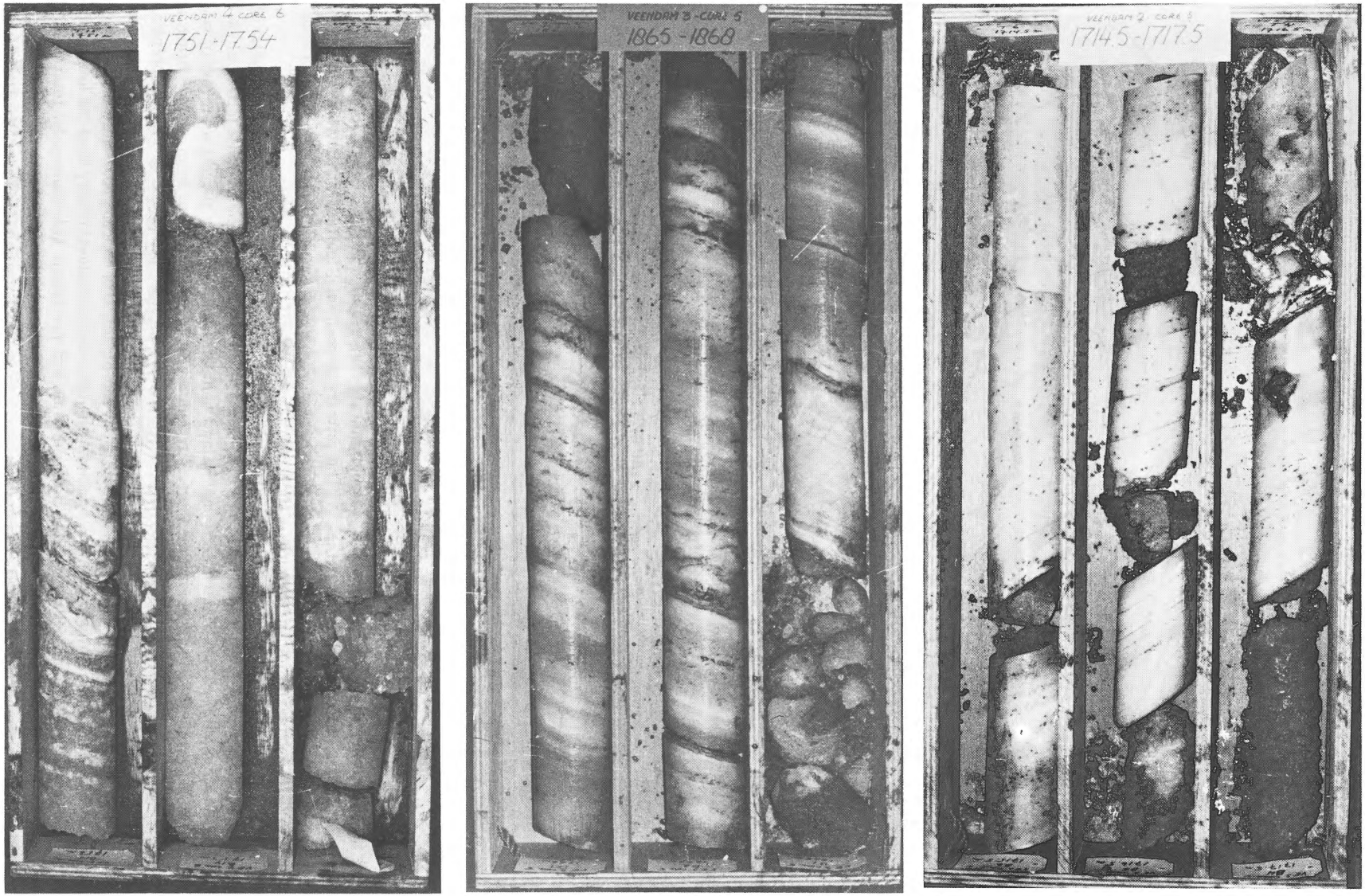

Fig. 7
Core photographs; the white parts consist of halite, the dark bands of carnallite (length of cores 1 m).

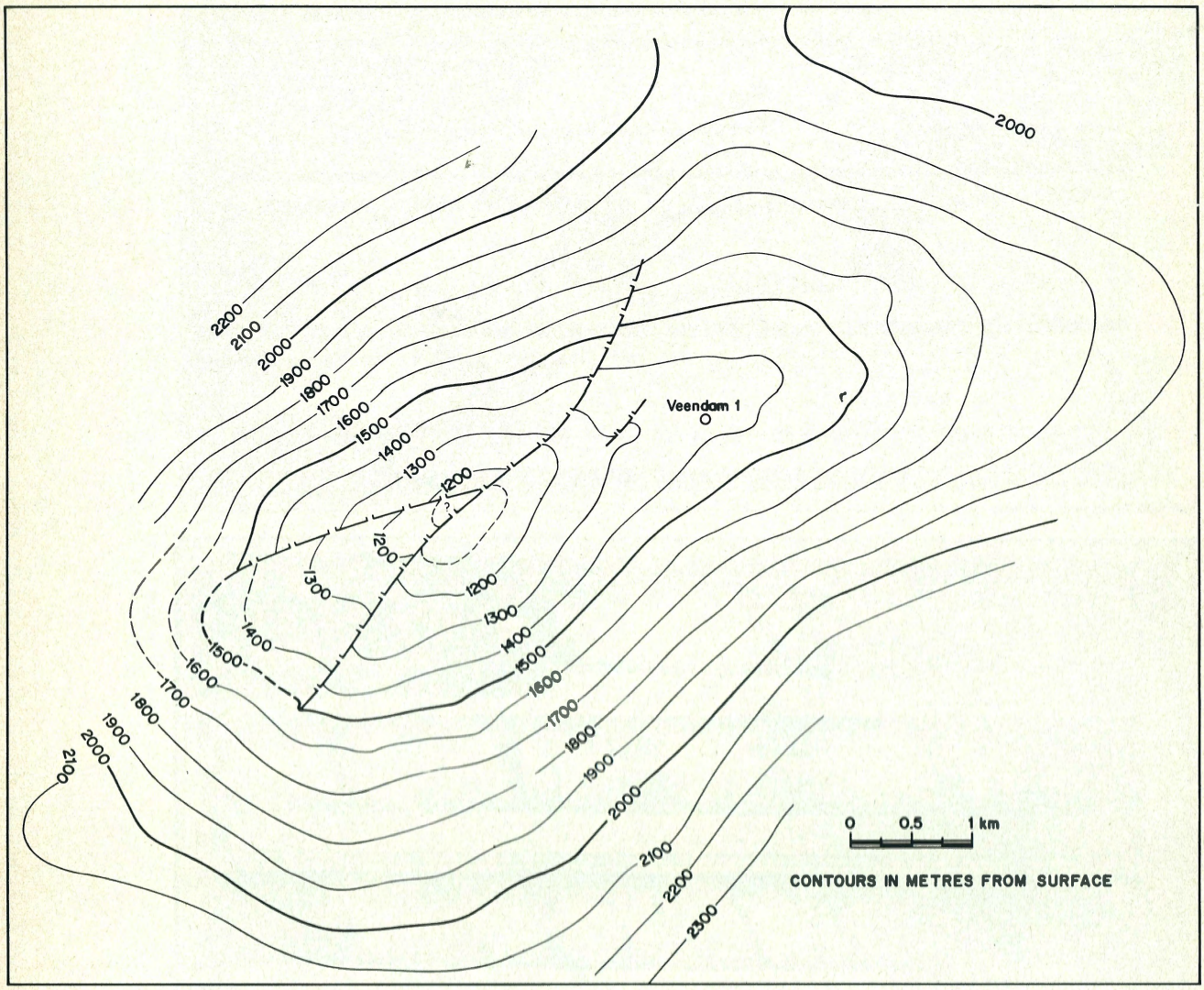

Fig. 8
Structural map of top Zechstein (Veendam structure).

Depositional environment

Primary depositional features differ distinctly between the two upper magnesium-salt subcycles Z-III-2 and 3 and the lowest one (Z-III-1); they are summarized in Table III.

The development of the Z-III-1-b magnesium-salt sequence conforms in principle with the physico-chemical model of static isothermal evaporation of normal seawater as described by BRAITSCH (1971). The repeated presence of bischofite in the drillholes proves the occurrence of full evaporation cycles. Numerous alternations of the bischofite and halite layers indicate a mechanism that regularly reversed the evaporation process. Presumably this was caused by intermittent influx of fresh (sea-)water with a subsequent drop in salinity. The phenomena of full static evaporation and development of relatively thin layers of simple composition are indicative of shallow water. Judging from the temperature table of primary precipitation by BRAITSCH (1971) (Table IV) the estimated kieserite/carnallite ratio for the Veendam Z-III-1-b would indicate temperatures in the range of 35-45°C.

The primary depositional features of the two upper carnallite horizons Z-III-2-b and Z-III-3-b have little in common with those of Z-III-1-b.

The indistinct bedding and weak development of cycles of Z-III-2-b and 3-b, together with the intimate mixing of carnallite and halite crystals, strongly suggest a process of co-precipitation. Since this cannot occur from a single brine, a deeper-water body must be postulated in which concentration stratification is present. In such a brine halite will precipitate from the higher, less concentrated stratum, and carnallite with higher concentration/density from the lower one. Both minerals will precipitate simultaneously. Intermittent influx of fresh (sea-)water into the water body would cause a temporary drop in concentration. However, the fresh, low-

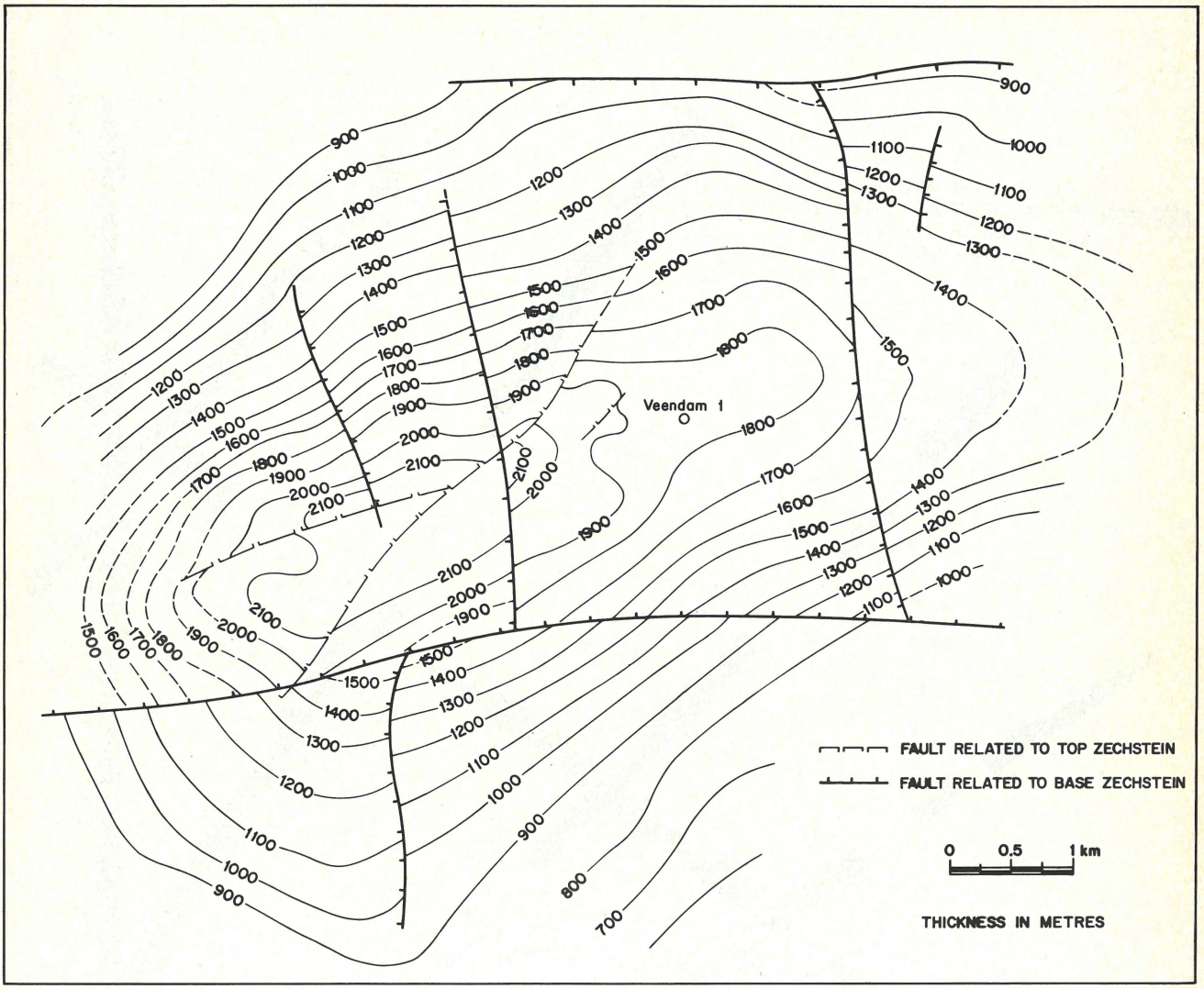

Fig. 9
Isopach map of the Zechstein (Veendam structure).

density water will not mix readily with the lower layers of higher density, so the event will not be characterized by a pronounced change in the composition of the precipitates. Changes do occur, as can be seen in the Veendam holes, but seldom are they developed into well-defined subcycles.

Structure

Seismic results of the 1975 survey covering the Veendam structure are shown on the top-Zechstein structural map (Fig. 8) and the Zechstein isopach map (Fig. 9). The structure is slightly elongated in a northeasterly direction, is slightly asymmetrical, and has a domeshaped roof and an almost flat bottom. The depth to the saltdome's top is 1150 m. Salt thickness decreases from 2100 m at the crest to 500 m on the flank, compared with an estimated depositional thickness of 900 m.

A large longitudinal normal fault was discovered extending along the crest of the structure with a displacement of approximaterly 70 m. The roof, however, seems affected relatively little and no indication of salt piercement into the overlying strata could be observed. Furthermore, the overlying Triassic strata appeared sufficiently thick to have preserved the salts from erosion and leaching during the period of non-deposition and erosion in the Jurassic.

Lateral prediction results

The applicability of seismic acoustic impedance processing, discussed in the following chapter, was confirmed. Magnesium-salt layers can be identified on seismic sections and their thickness measured. Minimum thickness detection limit of magnesium-salt layers is approximately 12 m.

Observed short-distance thickness variations (Fig. 10)

Fig. 10
Veendam structure; seismic interpretation of the thickness of Z-III-2-b + Z-III-3.

confirm the presence of magnesium-salt subpillows, but the density of data is insufficient for contouring. A detailed seismic survey later this year is designed to rectify this.

EXPLORATION TECHNIQUES

Oil exploration techniques (seismology, rotary drilling, petro-physical logging) are used in magnesium-salt exploration. Some of these techniques were adapted and are discussed below.

Lateral prediction

This seismic processing and interpretation method is used for the identification of buried magnesium-salt layers on seismic sections and for the determination of the thickness of these layers.

Introduction – In the seismic reflection method, a source of acoustic waves at the surface emits a wavelet or pulse at time = 0. The velocity with which this wavelet travels through the subsurface depends mainly on the following rock

properties:

(1) *lithology:* the velocity ranges from 6000 m/s in anhydrite to 1850 m/s in soft clay;
(2) *pressure:* due to compressability the velocity in a sandstone will increase when buried at greater depth; rock salt is non-compressible and does not show a velocity change with depth;
(3) *porosity:* higher porosity gives a lower velocity;
(4) *porefill:* a gas-filled rock shows a lower velocity than the same rock when water-filled.

Transmission of the wavelet cannot be described by velocity alone. In addition to propagation velocity, the acoustic impedance (A.I.) of the rock is needed to describe adequately the transmission process. The A.I. of the rock is the product of its acoustic velocity (V) and bulk density (ϱ).

At boundaries where the acoustic impedance changes, part of the wavelet is reflected in the form of an identical, but lower-amplitude wavelet. The reflected part is given by the reflection coefficient R:

$$R = \frac{V_2\varrho_2 - V_1\varrho_1}{V_2\varrho_2 + V_1\varrho_1} \quad (1)$$

where subscript 1 denotes the overlying, and 2 the underlying, material. A boundary with a positive R will reflect a wavelet with the same polarity as the incoming wavelet, which is reversed when R is negative.

Simple rearrangement of (1) gives:

$$V_2\varrho_2 = V_1\varrho_1 . \frac{1 + R}{1 - R} \quad (2)$$

Therefore, given the A.I. of the overlying material, and if R is measured accurately enough, the A.I. of the underlying material can be calculated.

Mathematical transformation of (1) leads to

$$\ln A.I._z = \int_0^z R + C \quad (3),$$

where C is a constant.

Thus the A.I. at depth Z can be found by integration of all reflection coefficients between the surface and Z. Formula (3) is easier to handle in computers.

However, accurate determination of R on a seismogramme is hampered by i.a. the following factors:

(1) the acoustic source emits only in a limited frequency range;
(2) the earth has a filtering effect on the wavelet; higher frequencies are attenuated more than lower frequencies and the effect increases with depth;
(3) the emitted wavelet is one-sided, starting at time $\tau = 0$, and therefore the received, reflected wavelets are also one-sided; the reflected wavelet is situated behind the actual reflection time of the interface. The recorded reflection is thus not symmetrical in relation to the reflecting boundary.

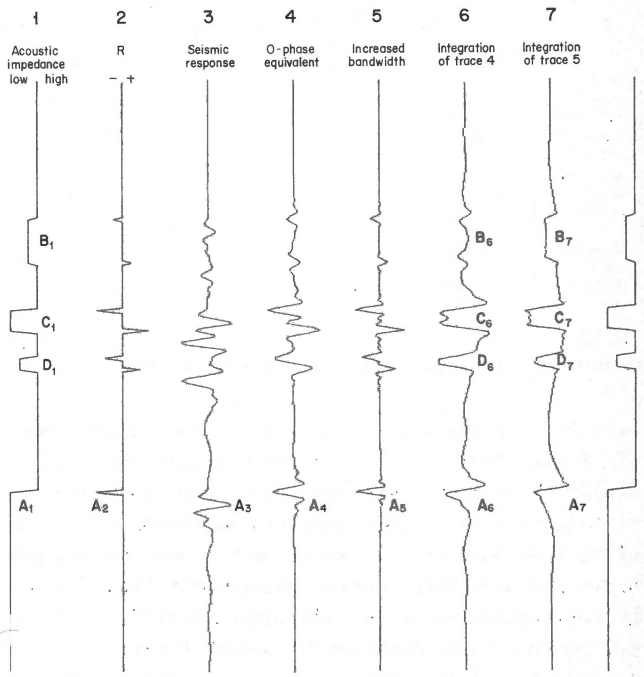

Fig. 11
Processing steps for seismics.

Because of these factors the wavelet is lengthened as it travels through the earth and thereby loses resolving power. The one-sidedness of the reflected wavelet moreover impedes correlation of its position and magnitude of maximum deflection with the position of the actual reflection boundary and the value of the reflection coëfficient.

Data processing – The various processing steps to correct this are given in figure 11.

At A2 an artificial reflection coefficient with value –3 is drawn, resulting from the decrease in A.I. as given in A1. At A3 the seismic expression of this reflection is found as it might be recorded in the field. Standard seismic data processing shortens the reflection expression, but will not change the one-sidedness. The most modern techniques, often referred to as wavelet processing, reshape the reflected wavelet so that it will be symmetrical with respect to the reflecting boundary (A4).

This reshaping is equivalent to zeroing the phase of the wavelet and is also called phase-deconvolution. The result is the symmetrical or zero-phase wavelet A4, which has the same frequency content as A3.

Improved vertical resolution is obtained through additional shortening of the wavelet by increasing the band width (frequency content), leading to A5. This step counteracts the filtering effect of the earth and has the same effect as improving the seismic source. This frequency boosting must be done carefully because the omnipresent noise will be amplified as well. Only that part of the frequency spectrum of the recorded and preprocessed data where the signal to noise

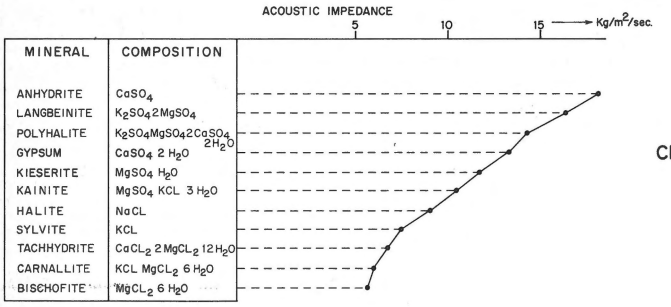

Fig. 12
Acoustic impedance values of some evaporite minerals.

ratio ≥ 1 will in general be suitable for this frequency booing. Especially the very low and high frequencies show generally a low signal to noise ratio. Consequently it is impossible to improve the resolving power of the wavelet to the level of the 'spike wavelet' (A2), which can be considered as equal to A4, with an infinitely improved bandwidth. The A.I. change which causes A2 can be computed via formula (3). Without amplitude deconvolution (frequency boosting, or step 4→5 in figure 11) the trace as given by A6 results. Integration of A5, however, gives A7, which is a better approximation of the impedance step. Although the deterioration of A6, as compared to A7, appears not too serious for this single step, reference to the whole of figure 11 shows differently for more complex configurations. At B1, C1, and D1 the acoustic impedance response of three layers with different thickness and A.I. is given; they could correspond, for instance, to sandstone layers with a porefill of water, gas, and oil respectively (from top to bottom), within a massive shale. Similar processing as described above demonstrates the merit of amplitude

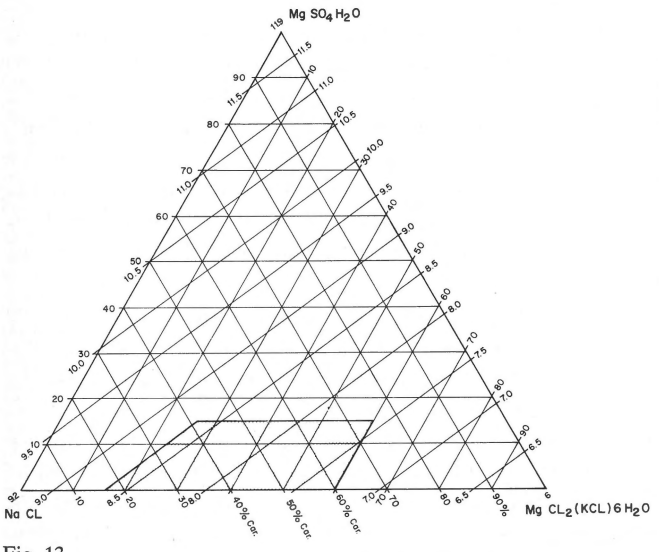

Fig. 13
Diagram to determine the A.I. values of mixtures of carnallite, kieserite and halite. The shaded area shows the range of compositions as found in the drill holes, which is detectable on the A.I. sections.

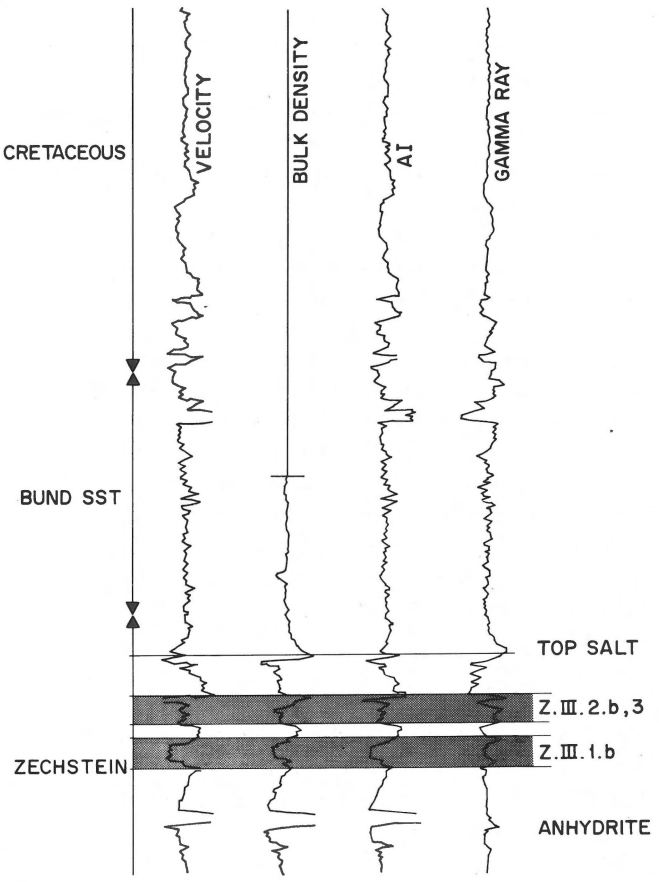

Fig. 14
Acoustic impedance log, derived from density and velocity logs, and compared with gamma-ray log. The latter is used to distinguish between carnallite and bischofite.

deconvolution: B7 is a clear, low-impedance layer, not easily recognized in B6; D6 has a lower impedance than C6, while in reality the reverse is true, as is shown in trace 7. The thickness of the layer is also easier to determine on trace 7 than on trace 6.

Accurate thickness determination of geological layers from seismic data must therefore incorporate the following steps:

(1) determination of the wavelet which is present in the seismic recording at the level of our objective;
(2) phase deconvolution in order to change the shape of the recorded reflection and make it symmetrical around the actual position of the reflecting boundary;
(3) amplitude deconvolution in order to conteract the filtering effect of the earth, and to improve the bandwith of the received signal. This deconvolution must take into account the signal to noise ratio versus frequency for optimum resolution improvement;
(4) integration of the deconvolved data to arrive at an A.I. trace. The acoustic impedance section which is obtained in this way can be regarded as band limited (no high and low frequencies) A.I. logs of wells drilled along the seismic line.

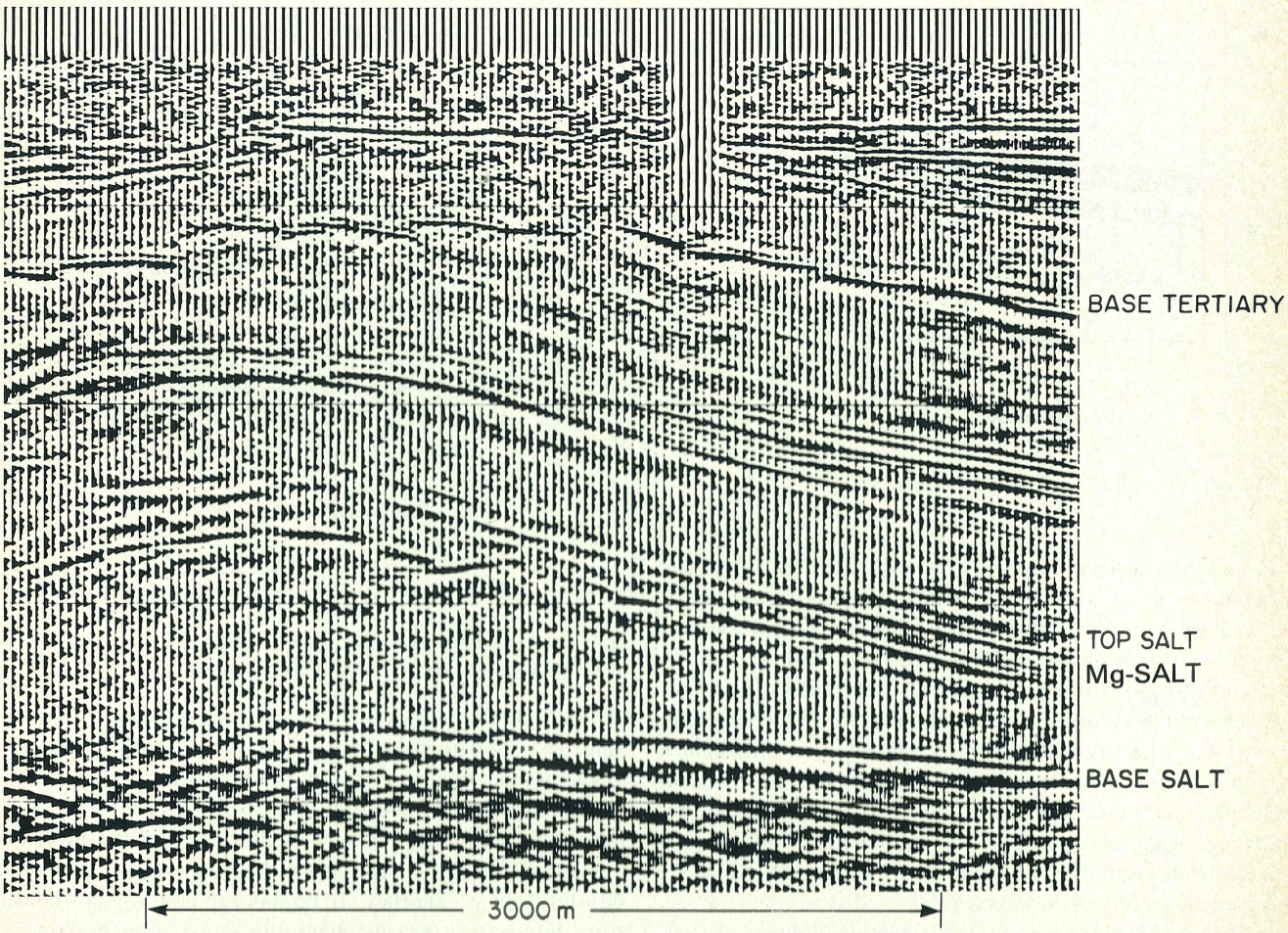

Fig. 15
Migrated acoustic impedance section of the Veendam structure.
Vertical scale to base salt 1.9 ms (± 3000 m).

Lithological units, including magnesium salts, can then be recognized, and layer thicknesses determined on each trace. Ideally, also the relative A.I. can be measured.

Lithological parameters – At Veendam the rock type hosting the magnesium salts is halite. The relative A.I. measured is translated into the A.I. difference between pure halite and impure magnesium salt; this determination provides a measure of the carnallite/bischofite content or grade of the ore layer.

Theoretical values of the A.I. of different evaporite minerals are shown in figure 12. The A.I.'s of carnallite and bischofite are significantly lower than for halite; for kieserite the reverse applies.

The magnesium-salt layers always contain halite while kieserite is nearly always present in varying amounts. Therefore the A.I. of mixtures of these components should be taken into account, when the measured A.I. differences are translated into carnallite content of the layer (Fig. 13).

It can be seen that a content of up to 15% kieserite will not disturb the 'visibility' of the magnesium-salt layers, provided the carnallite-bischofite content is higher than 40%.

Calibration – The acoustic-velocity (sonic) and bulk-density logs recorded in a borehole were combined to form an A.I. log (Fig. 14). Because the A.I. values of the borehole were recorded as a function of depth, conversion must be carried out from the depth-domain to the time-domain, using information from the acoustic velocity logs. The A.I. values can now be presented as a function of the two-way reflection time. Subsequently, the low and high frequencies are removed from the time-domain log by filtering, thus achieving a bandwidth identical to the one obtained for the seismic data after amplitude deconvolution. The final log is now directly comparable to the processed seismic sections.

This procedure provides the opportunity of checking the processing results and calibrating the final seismic data with the information from a drillhole.

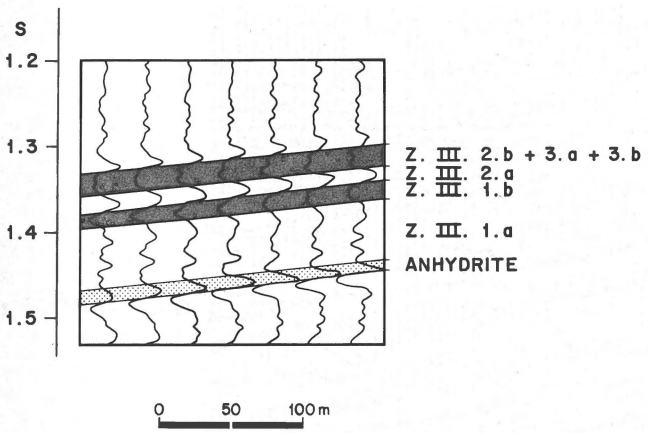

Fig. 16
Example of working scale of A.I. section.

Results and Interpretation – Figure 15 gives the final impedance section. The magnesium-salt layers recognized in the drillhole are indicated. Presentation of this section on a more workable scale (1 : 3000 horizontal and 20 cm/s reflection-time vertical scale) permits determination of both layer width and maximum deflection of the reflection of the ore layer on every trace (Fig. 16). The width in time units is converted to thickness in metres by multiplication with the velocity; the maximum deflection is assumed to indicate the average grade of the ore layer at that location. Both readings have been combined in figure 10 as bargraphs along the seismic lines of the 1975 survey.

The resulting information on the combined upper two carnallite layers shows distinct short-distance variation in thickness, not amenable to contouring on this line-spacing. The open spaces on the lines represent sections of poor reflection caused by adverse conditions; as drilling proved subsequently, they do not necessarily mean absence of carnallite horizons.

Migration

Migration is the process used to reconstruct the actual positions of reflection points, which on dipping strata do not occur below their measuring points. In this way subpillows can be located accurately in relation to the surface which is essential for the correct positioning of production holes.

The raypath between reflection and measuring points is generally not a straight line; deviations are caused by refraction at velocity boundaries and curvature due to gradual velocity changes. Moreover, the raypath will in general not be vertical at the surface but reach the measuring point under an angle with the vertical.

Constructing an accurate vertical seismic section requires plotting every reflection point at its true position in the subsurface. It can be imagined as a reconstruction of the raypaths between measuring points and reflection points

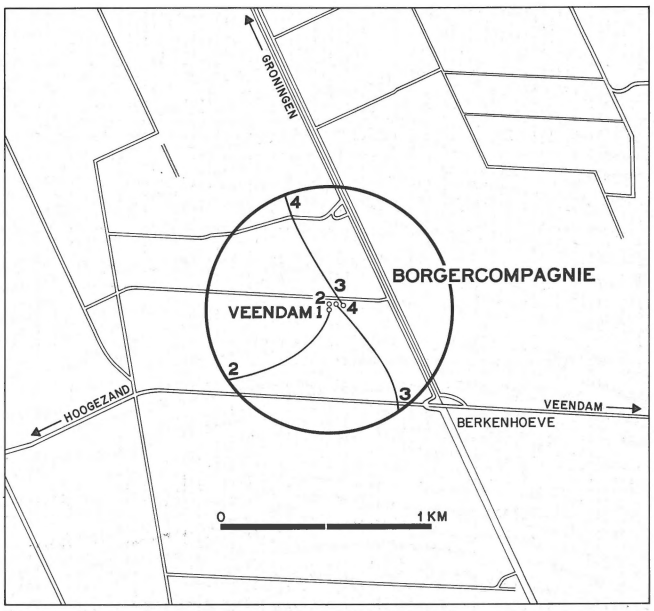

Fig. 17
Relationship between petrophysical measurements and core data of part of the Zechstein III-2-b in bore-hole Veendam 2.

through all the refractions and curvatures which occur at velocity boundaries, etc. This requires good knowledge of velocities and velocity distributions. Moreover, complete reconstruction is possible only in a 3-dimensional way. For instance, a seismic line may be measuring along the strike of one interface, and at the same time be measuring in the dip-direction of another. If no information was available from intersecting seismic lines, the apparently horizontal boundary of the first interface could not be migrated while the exact position of the dipping reflector could be found (horizontal interfaces are not shifted during the migration process).

The amount of cross-line information required is inversely proportional to the objective's size and the structure's complexity.

Calculation of the maximum spacing of subsurface reflection points which enables an accurate migration and mapping of the ore layers of the Veendam salt pillow and its expected carnallite subpillows gives a figure of 20 m.

Forthcoming seismic survey

The area under consideration for the initial period of brine production (3 × 4 km) will be covered by this 3-D seismic survey with subsurface reflection points on a 20 × 20 m grid. The subsequent data processing will incorporate i.a. velocity determinations from the seismic data, 3-dimensional migration, conversion to acoustic impedance, etc. As an illustration of the size of the data-processing task it must be realized that for each properly 3-D-migrated subsurface point the information of some 3500 seismic traces must be combined (an area with a radius of 700 m). This must be performed for

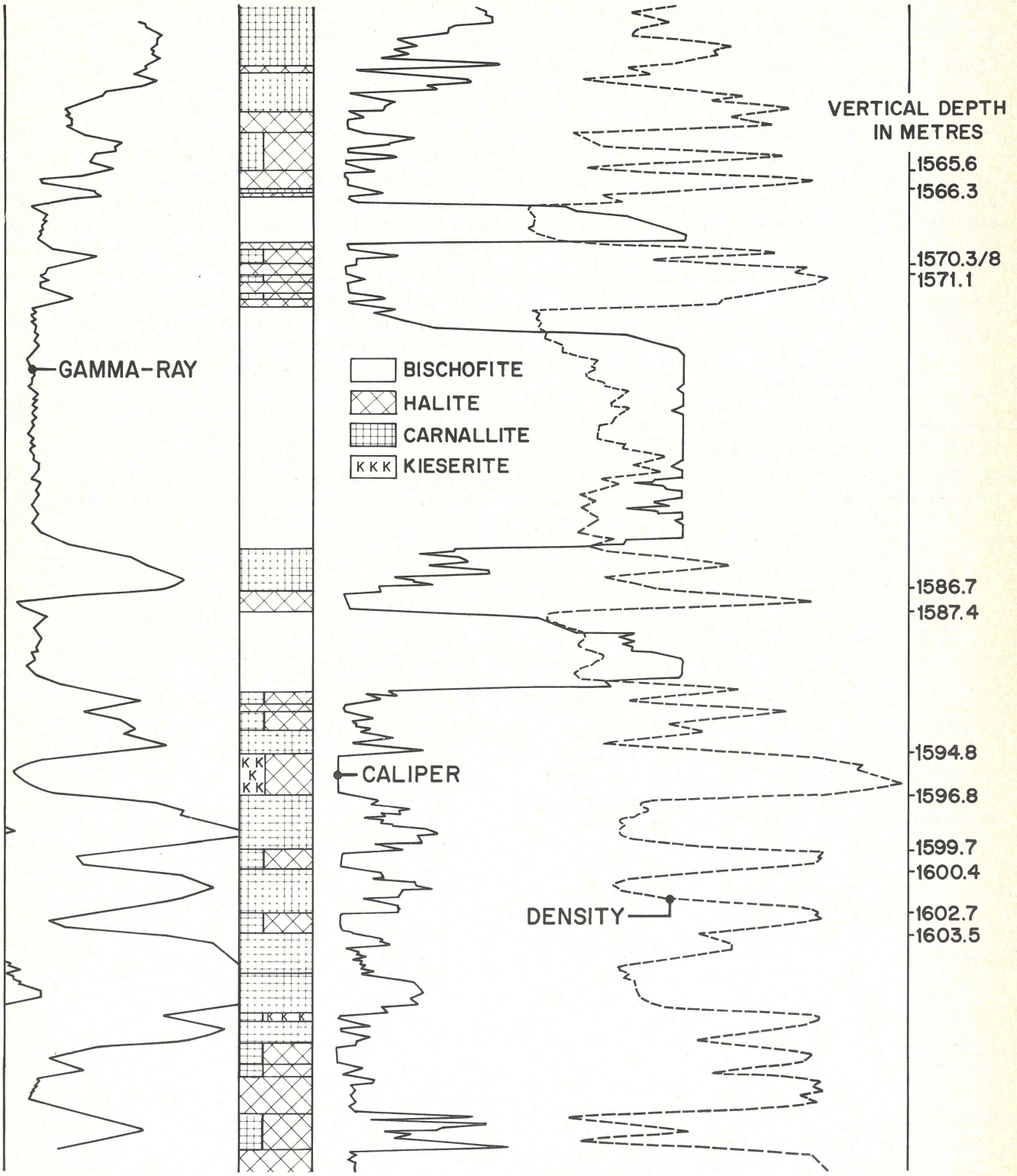
VERTICAL DEPTH
IN METRES
1565.6
1566.3
1570.3/8
1571.1
1586.7
1587.4
1594.8
1596.8
1599.7
1600.4
1602.7
1603.5
GAMMA-RAY
BISCHOFITE
HALITE
CARNALLITE
KIESERITE
CALIPER
DENSITY

Table V
Main characteristics of salt-composing minerals.

Mineral	Density g/cm³	Gamma ray intensity	Hole diameter
Halite (NaCl)	2,17	low	not enlarged
Carnallite ($KCl.MgCl_2.6H_2O$)	1,60	high	enlarged
Bischofite ($MgCl_2.6H_2O$)	1,57	low	very large
Kieserite ($MgSO_4.H_2O$)	2,57	low	not enlarged
Sylvite (KCl)	1,99	very high	not enlarged

every subsurface point of the 20 × 20 m grid. Some 250,000 seismic traces will be measured and processed into approximately 600 km of 3-D migrated, acoustic impedance section for subsequent interpretation.

Petrophysics

Petrophysical well logs are run before installing the 10³/₄″ casing and after coring. For determination of the rock type, formation density, natural gamma-ray and sonic logs are recorded, together with a caliper run to determine hole diameter. Table V illustrates the main characteristics of the minerals that compose the bulk of the salt.

Figure 17 shows a typical section of the lower magnesium-salt layer in VE-2. The composite well log shows the gamma-ray, caliper, and bulk density readings, combined with the lithological interpretation.

Petrophysical logs provide a rapid and cost-effective method of determining ore composition and grade. Small-scale structural and stratigraphic data are obtained from the cores which are used also to calibrate the logs.

REFERENCE

Braitsch, O. 1971 Salt deposits, their origin and composition – Springer Verlag (Berlin).